Applied Catalysis B: Environmental 138–139 (2013) 318–325

Contents lists available at SciVerse ScienceDirect

Applied Catalysis B: Environmental

journal homepage: www.elsevier.com/locate/apcatb

Sonophotocatalytic mineralization of antipyrine in aqueous solution

A. Durán*, J.M. Monteagudo, I. Sanmartín, A. García-Díaz

Department of Chemical Engineering, Grupo IMAES, Escuela Técnica Superior de Ingenieros Industriales, Instituto de Investigaciones Energéticas y Aplicaciones Industriales (INEI), Universidad de Castilla-La Mancha, Avda. Camilo José Cela 3, 13071 Ciudad Real, Spain

ARTICLE INFO

Article history:
Received 15 November 2012
Received in revised form 18 February 2013
Accepted 8 March 2013
Available online 15 March 2013

Keywords:
Emerging contaminant
Pharmaceuticals
TOC
Ultrasound
UV radiation

ABSTRACT

The mineralization of aqueous solutions of antipyrine, an emerging contaminant, using an innovative homogeneous sono-photocatalytic oxidation process (H_2O_2/UV/Fe/Ultrasound) was evaluated in an artificial UV lamp.

At the selected operation conditions [H_2O_2] = 1500 ppm, pH = 2.7, amplitude = 100%, pulse length (cycles) = 0.3 during 15 min and then 1, 92% of TOC is removed after 50 min treating an aqueous solution containing 50 ppm of antipyrine. An important synergistic effect between sonolysis and photoFenton (UV/H_2O_2/Fe) of 45.4% was quantified using the first order rate constants for TOC.

Comparison experiments of scavenger-loaded conditions demonstrate that the antipyirine photodegradation proceeds mainly through a radical mechanism probably beginning by the cleavage of the N—N bond of penta heterocycle leading to the formation of aromatic acids (anthranilic and 1,4-benzenedicarboxylic acids) then followed by the opening of phenyl ring to form small molecular organic acids (mainly 2-butenedioic, 4-oxo-pentanoic and butanedioic acids), which may be decomposed further into CO_2.

1. Introduction

The US EPA (United States-Environmental Protection Agency) defines emerging contaminants (ECs) pollutants as new chemicals without regulatory status and which impact on environment and human health are poorly understood. ECs must be removed within an objective of quality and preservation of good ecological status of water by 2015, but authorities should pay particular attention to their industrial discharge into the water. Among ECs, numerous studies have demonstrated the presence of pharmaceuticals in urban wastewater, sewage from hospitals and surface waters [1,2]. They have also been detected in groundwater and even in some drinking water [3–5] and they can also reach the soil due to the use of wastewater for irrigation [6].

A recent review of data on ECs concentrations in wastewater, in influent and effluent from wastewater treatment plants (WWTPs) showed that although the concentration of antipyrine was relatively low (0.04 μg/L), it remained very resistant to treatment (32.5% of removal rate) [7]. Reusable water should be free of these persistent toxic non-biodegradable substances [8], so that a tertiary effective treatment is required.

Sonophotocatalysis, which involves the use of a combination of ultrasonic sound waves, ultraviolet radiation and a catalyst is becoming an alternative, low-cost, effective and innovative water treatment method [9,10]. Ultrasonic sound waves in the range of 20–100 kHz are transmitted through the aqueous solution to create an "acoustic cavitation". The heat generated by the cavity implosion decomposes water into extremely reactive hydrogen atoms and hydroxyl radicals, that can recombine during cooling to form hydrogen peroxide and molecular hydrogen.

If ferrous ions are added to the solution, they react with ultrasonically generated H_2O_2, thus, enhances the production of •OH radicals, which can be readily used for pollutant degradation. The accelerating effect on mineralization of adding H_2O_2 under ultrasonic irradiation is due to the additional decomposition of H_2O_2 into •OH radicals under extreme conditions [11].

In a previous work, homogeneous sonophotolysis of industrial wastewater coming from food processing industry has successfully been tested using ultrasonic sound waves, UV radiation and H_2O_2 in an homogeneous process [10]. The synergistic effect of this combination and the effect of operation parameters in the reduction of Total Organic Carbon (TOC) and toxicity were studied.

This work is focused on the mineralization of aqueous solutions of antipyrine, an emerging contaminant, using a rising homogeneous sono-photocatalytic oxidation process (UV/H_2O_2/Fe(II)/US).

Experimental tests based on a factorial design were analyzed and results were fitted using neural networks (NNs), which allowed

Abbreviations: ECs, emerging contaminants; k_m, mineralization rate constant; NNs, neural networks; TOC, total organic carbon; US, ultrasound; US EPA, United States-Environmental Protection Agency; UV, ultraviolet; WWTPs, wastewater treatment plants.

* Corresponding author. Tel.: +34 926295300x3814; fax: +34 926295361.
E-mail address: Antonio.Duran@uclm.es (A. Durán).

0926-3373/$ – see front matter © 2013 Elsevier B.V. All rights reserved.
http://dx.doi.org/10.1016/j.apcatb.2013.03.013

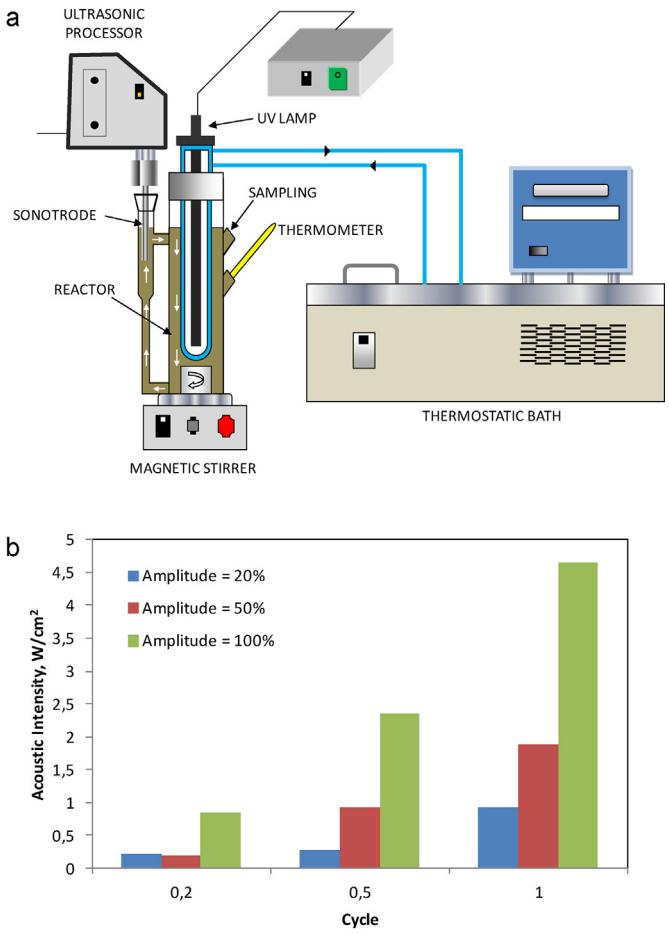

Fig. 1. (a) Experimental set-up. (b) Acoustic intensity measured at cycle value ranging from 0.2 to 1, at amplitudes of 20%–100%.

the value of the mineralization rate constant (k_m) to be estimated within the studied range as a function of the operating variables (initial concentrations of H_2O_2 and Fe(II) amplitude and pulse length). The synergistic effect between sonolysis and photoFenton process, as well as the mechanisms involved during mineralization were also studied.

2. Experimental

2.1. Materials

Antipyrine (99%) was obtained from Acros. 30% hydrogen peroxide (H_2O_2) were purchased from Merck and used as received. The pH of the wastewater in each test was adjusted with H_2SO_4 and NaOH solutions.

For experimental runs focused on the evaluation of kinetic mechanism, 2 different radical scavenger were added to the system (KI and t-butyl alcohol) [12].

2.2. Experimental runs and analysis

All experiments were carried out at pH = 2.7 in a 400-mL stirred photoreactor (Fig. 1a) with an external jacket connected to a thermostatic bath to maintain a constant temperature (30 ± 0.5 °C). A Heraeus TQ150 UV Hg immersible lamp with a nominal output of 150 W emitting at λ = 190–280 nm was used to irradiate the solutions.

A 24 kHz, 200 W direct inmersion horn sonicator (UP200S with an S14 sonotrode, Hielscher, with a 1.4 cm diameter stainless steel probe) was used to generate ultrasonic sound waves in the sonoreactor. The amplitude of the oscillatory system (power output) can be steplessly adjusted between 20% and 100%. The pulse mode factor (cycles) can be continuously varied between 10% and 100%. The set value equals the acoustic irradiation time in seconds, the difference to one second is the pause time. Thus, a setting of 1 implies that it is continuously switched on, whereas a setting of 0.6 means a power discharge of 0.6 s and a pause of 0.4 s.

UV absorption spectra were determined using a UV-vis spectrophotometer (HACH-LANGE, model DR5000)

Total organic carbon concentration was determined using a TOC analyzer (Shimadzu TOC-5000A). Monitoring of the H_2O_2 concentration in solution was by titration with an aqueous solution of potassium permanganate (0.02 mol/L) using an automatic Titrino.

Mass spectrometry (MS) was performed using a TOF-MS micrOTOF-Q II (Bruker Daltonics Inc., Billerica, MA, USA) equipped with a 2.5 mL or 500 μL Hamilton gastight syringe (Hamilton, Reno, NV, USA) delivered the sample and calibrant solution with electrospray ionization source and negative–ion polarity. MS measurements were taken over the range $50 < m/z < 600$.

2.3. Experimental design

A central-composite experimental design was applied to investigate the effects of four variables, initial concentrations of H_2O_2 and Fe(II), amplitude and pulse length on the response function, the mineralization rate constant. The design process consisted of three series of experiments:

(i) a factorial design with 2^k trials (all possible combinations of codified values +1 and −1), which in the case of $k = 4$ variables consisted of 16 experiments
(ii) selection of the axial distance of the star points (codified values $\alpha = 2^{k/4} = \pm 2$) consisting of $2k = 8$ experiments, and
(iii) replicates of the central point (three experiments).

The complete experimental design and additional experiments performed to obtain optimal conditions, including variable ranges, are shown in Table 1.

2.4. Neural-network strategy

The neural network (NN) applied in this work was solved with two neurons, using a simple exponential activation function and a solution strategy based on a back-propagation algorithm. Parameters were fitted using the solver tool in a custom spreadsheet in Microsoft Excel using a nonlinear fitting method. Further details can be found in the literature [13]. The input variables in this study were the initial concentration of H_2O_2 and Fe(II), amplitude and pulse length (cycles). Temperature was not controlled during tests, but it was measured and its medium values were also added to the fitting. The response function was the mineralization rate constant. Finally, a measure of the saliency of the input variables was made based on the connection weights of the neural networks. This study analyzed the relevance of each variable with respect to the others (expressed as percentages).

3. Results and discussion

3.1. Ultrasonic power measurement: calorimetry

The acoustic intensity of different ultrasound setting employed was measured by standard calorimetric method [14,15]. Deionized water was used as a substitute for the antipiryne solution because the mass fraction of water to antipiryne solids was negligible. The

Table 1
Experimental design for the sonophotocatalytic degradation of antipyrine.

Factorial design					Response function
Experiment	**[H_2O_2], (ppm)**	**[Fe (II)], ppm**	**Amplitude, %**	**Pulse length**	**Mineralization rate constant, min^{-1}**
1	812.5	8	80	0.8	0.067
2	437.5	8	80	0.8	0.054
3	812.5	4	80	0.8	0.039
4	437.5	4	80	0.8	0.053
5	812.5	8	40	0.8	0.042
6	437.5	8	40	0.8	0.044
7	812.5	4	40	0.8	0.031
8	437.5	4	40	0.8	0.039
9	812.5	8	80	0.3	0.048
10	437.5	8	80	0.325	0.042
11	812.5	4	80	0.325	0.041
12	437.5	4	80	0.325	0.018
13	812.5	8	40	0.325	0.041
14	437.5	8	40	0.325	0.041
15	812.5	4	40	0.325	0.020
16	437.5	4	40	0.325	0.034
17	1000	6	60	0.55	0.035
18	250	6	60	0.55	0.044
19	625	10	60	0.55	0.042
20	625	2	60	0.55	0.025
21	625	6	100	0.55	0.060
22	625	6	20	0.55	0.041
23	625	6	60	1	0.057
24	625	6	60	0.1	0.048
25	625	6	60	0.55	0.066
26	625	6	60	0.55	0.057
27	625	6	60	0.55	0.061
Additional experiments (for determination of optimum conditions)					
28	1368.2	17.95	100	1	0.064
29	731.8	17.95	100	1	0.061
30	1368.2	8.05	100	1	0.069
31	731.8	8.05	100	1	0.065
32	1500	13	100	1	0.076
33	600	13	100	1	0.044
34	1050	20	100	1	0.064
35	1050	6	100	1	0.058
35	1050	13	100	1	0.068
Additional experiments (for determination of the effect of cycles and dosage)					
36	1500	12	100	1	
37	1500	12	100	0.3/1	Cycles: 0. 3 for 15 min, then 1
38	1500 + 1500	12	100	0.3/1	Two additions of H_2O_2
39	300* + 1200**	12	100	0.3/1	* Initial addition/** dosified
40	300* + 1200**	12	100	0.3/1	* Initial addition/** dosified
41	300* + 1200**	12	100	1	* Initial addition/** dosified
Additional experiments (for determination of synergistic effects)					
42	1500	–	–	–	No radiation, no Fe, no sonication
43	1500	–	–	–	No Fe, no sonication
44	1500	–	100	0.3/1	No Fe, no H_2O_2
44	1500	–	100	0.3/1	No Fe, no radiation
46	1500	12	–	–	No radiation, no sonication
47	1500	–	100	0.3/1	No Fe
48	1500	12	–	–	No sonication
49	1500	12	100	0.3/1	No radiation

ultrasonic power actually entering the system may now be obtained according to equation:

$$\text{Power input}, \quad q = mc\frac{dT}{dt} \tag{1}$$

In this equation, m is the mass of water; c is the heat capacity of water and dT/dt is the temperature gradient over time. The acoustic intensity (W/cm^2) was determined by dividing the power input (q) by the sonotrode surface area (A) according to equation:

$$\text{Acoustic intensity} = \frac{q}{A} \tag{2}$$

The cycle regulate the value of the pulse length. The set value equals the acoustic irradiation time in seconds, the difference to 1 s is the pause time. A cycle value of 1 is also known as the CW mode. The amplitude percentage indicates the percentage of wattage that is being input into the system.

Fig. 1b shows the acoustic intensity at amplitudes of 20, 50 and 100% with cycle values ranging from 0.2 to 1.

3.2. NN fitting

The experimental results obtained for the mineralization constant were fitted with NNs, resulting in an average error of less than 10%. The equation and fitting parameters are shown in Table 2. N_1 and N_2 are general factors related to the first and the second neurons, respectively. W_{11} to W_{15} are the contribution parameters to the first neuron and represent the influence of each of the variables in the process (initial concentrations of H_2O_2 and Fe(II), amplitude and pulse length and medium temperature, respectively); W_{21} to

Table 2
Equation and parameters for the NN fitting.

NN fitting*
Mineralization constan $t\,(\mathrm{min}^{-1}) = N_1 * (1/(1 + 1/\mathrm{EXP}([H_2O_2] * W_{11} + [Fe(II)] * W_{12} + Amplitude * W_{13} + \mathrm{Cycles} * W_{14} + \mathrm{Temperature} * W_{15}))) + N_2 * (1/(1 + 1/\mathrm{EXP}([H_2O_2] * W_{21} + [Fe(II)] * W_{22} + \mathrm{Amplitude} * W_{23} + \mathrm{Cycles} * W_{24} + \mathrm{Temperature} * W_{25})))$

Neurons and weight factors	Parameters	Values of neurons and factors to obtain the mineralization constant
N_1	Neuron	−0.0584
W_{11}	$[H_2O_2]$	−3.1893
W_{12}	[Fe(II)]	3.4183
W_{13}	Amplitude	−0.6520
W_{14}	Pulse length (cycles)	−0.2526
W_{15}	Temperature	−0.7263
N_2	Neuron	0.0759
W_{21}	$[H_2O_2]$	−3.5036
W_{22}	[Fe(II)]	7.4354
W_{23}	Amplitude	2.5037
W_{24}	Pulse length (cycles)	1.8695
W_{25}	Temperature	−1.8306

Saliency analysis (%)

$[H_2O_2]$	[Fe(II)]	Amplitude	Pulse length	Temperature
31.45	44.44	11.64	7.13	5.34

* Parameter values ($[H_2O_2]$, [Fe(II)], amplitude, pulse length and temperature) were previously normalized to the (0,1) interval.

W_{25} are the contributions to the second neuron corresponding to the same variables.

The results of a saliency analysis on the input variables for each neural network (%) are also shown in Table 2. From these results, it was possible to deduce the effect of each parameter on the mineralization degree. Thus, it was confirmed that the mineralization process was mainly influenced by hydrogen peroxide and Fe(II) initial concentrations (31.4 and 44.4% respectively), although the effect of the ultrasound waves is also important as will be explained below (amplitude with 11.6% and cycles with 7.13%).

3.3. Mineralization study

3.3.1. Effects of initial concentrations of H_2O_2 and Fe(II)

After an initial fitting, the factorial design was extended with additional experiments (28–35 in Table 1) increasing the upper limit of initial concentrations of hydrogen peroxide (from 1000 to 1500 ppm) and Fe(II) (from 10 to 20 ppm) to find the optimum operation conditions. In this way a definitive fitting was made (Table 2). Equation and parameters in this table enabled a simulation analysis of the effect of the studied variables on the value of the mineralization constant. Thus, the influence of $[H_2O_2]$ and [Fe(II)] on k_m were determined, as shown in Fig. 2a (simulation conditions at central values: $T = 31.95\,^{\circ}C$, amplitude = 60%, pulse length = 0.55).

The results showed that mineralization continuously increased with peroxide concentration (as more •OH radicals are formed due to photolysis of H_2O_2) until reaching a maximum, which highly depends on Fe(II) initial concentration. However, an excess of hydrogen peroxide also reacts with •OH radicals reducing the amount of radicals available to destroy antipyrine and decreasing the mineralization activity This effect, known as *scavenger effect*, also includes decomposition of hydrogen peroxide to form water and oxygen [13].

On the other hand, increasing concentrations of Fe(II) improves the mineralization constant value via the following reaction:

$$Fe^{(II)} + H_2O_2 \rightarrow Fe^{(III)} + {}^{\bullet}OH + OH^- \quad (3)$$

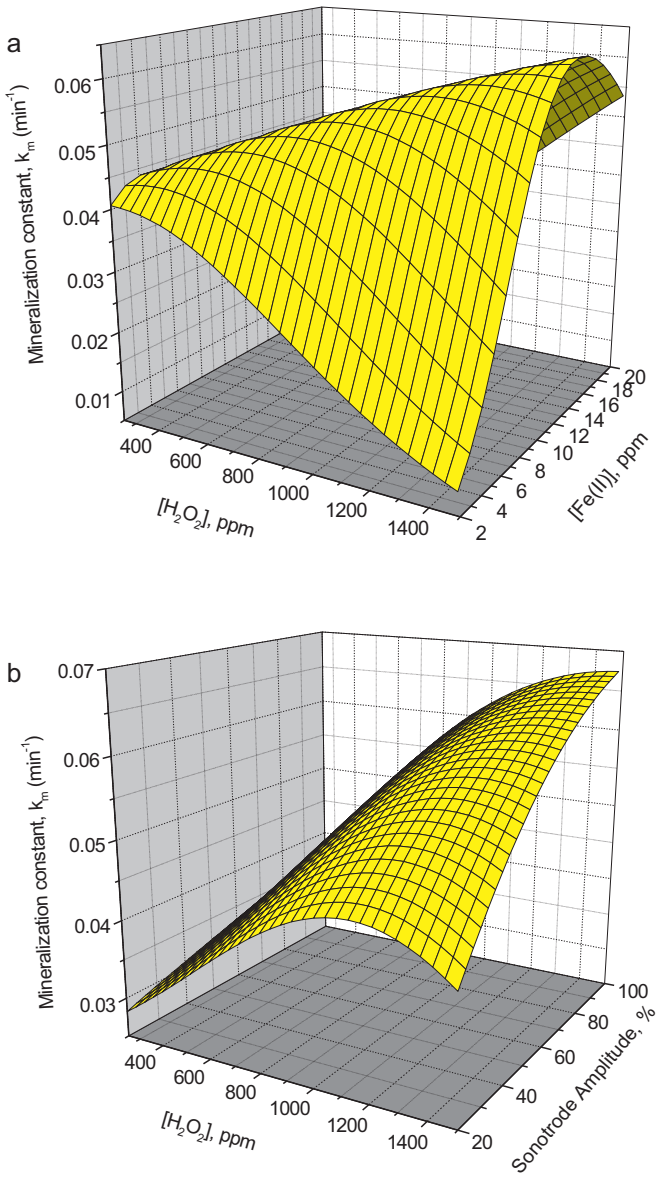

Fig. 2. (a) Effect of $[H_2O_2]$ and [Fe(II)] on the mineralization constant. Simulation at central conditions: $T = 31.95\,^{\circ}C$, amplitude = 60%, pulse length = 0.55. (b) Effect of $[H_2O_2]$ and amplitude of the sonotrode probe on the mineralization constant. Simulation at central conditions: $T = 31.95\,^{\circ}C$, [Fe(II)] = 11 ppm, pulse length = 0.55.

but an excess in Fe(II) reduces •OH radicals available for antipyrine elimination and decreases the observed kinetic constant via reaction

$$Fe^{(II)} + {}^{\bullet}OH \rightarrow Fe^{(III)} + OH^- \quad (4)$$

It can be said that the use of Fenton reagent in conjunction with ultrasound is beneficial only till an optimum loading and where the free radical attack is the controlling mechanism of destruction [16]. The maximum degradation is reached under the following conditions: $[H_2O_2] = 1500$ ppm and [Fe] = 12 ppm.

3.3.2. Effect of the amplitude of vibration of the sonotrode source

Fig. 2b shows the influence of the amplitude of sonication on the mineralization constant at the central values of the other parameters (simulation conditions: $T = 31.95\,^{\circ}C$, [Fe(II)] = 11 ppm, pulse length = 0.55). It can be seen that an increase in amplitude enhances significantly the mineralization rate due to a synergistic effect that

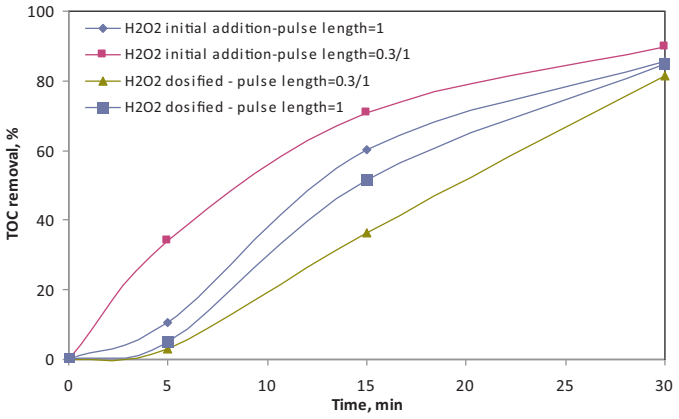

Fig. 3. Effect of dosage and pulse amplitude on the mineralization degree. Conditions: $[H_2O_2]$ = 1500 ppm, [Fe(II)] = 12 ppm, amplitude = 100, pulse length = 0.3 (during 15 min) and 1 later.

will be studied below. It is again confirmed that optimum conditions require 1500 ppm of hydrogen peroxide.

3.3.3. Effects of the pulse length and H_2O_2 dosage

After a thorough study of results, it was determined that increasing cycles had a negative effect at the beginning of reaction, but a positive effect later. Generally, it is accepted that the generation of highly reactive species such as hydroxyl (•OH), hydrogen (H•), hydroperoxyl (HO_2•) radicals and hydrogen peroxide are formed under the extreme conditions from the cavity implosion of ultrasonics waves [17,18]. Approximately 10% of the radicals generated in the bubble can diffuse into the bulk solution [19,20]. Thus, a possible excess of radicals could be generated at the early stages of reaction and this could negatively influence the mineralization rate. Accordingly, a new set of experiments (36–41 in Table 1) was planned decreasing the pulse length during the first 15 min to a value of 0.3 to set it to a value of 1 after that time. Fig. 3 shows an important improvement in the mineralization removal when this procedure is applied.

However, dosage of the optimal amount of hydrogen peroxide during 50 min after an initial addition of 300 ppm yields opposite results (Fig. 3). It can be deduced that the great number of cavitation bubbles generated at high acoustic intensities at the early stages of reaction (100% amplitude and high pulse length) may act as a barrier to the successful transfer of acoustic energy through the liquid [21]. Thus, sonication can lead to liquid agitation instead of cavitation with a poor transmission of the ultrasound through the liquid media. The key is then to reduce the pulse length, but not to decrease hydrogen peroxide concentration.

The following operation conditions were selected as optimal from the mineralization of antypirine: $[H_2O_2]$ = 1500 ppm, [Fe(II)] = 12 ppm, amplitude = 100, pulse length = 0.3 (during 15 min) and 1 later. Under these conditions, 92% of TOC is removed after 50 min and in total, 14 moles of H_2O_2 were consumed per each mol of total organic carbon removed from solution.

3.3.4. Effect of temperature

The utilization of an ultrasonic probe leads to an increase in bulk temperature. If the temperature is not controlled some undesired effects can occur (degradation of compounds of interest, volatilization of low volatile analytes, and even the physical characteristics of the liquid media may change in such a way that the ultrasonic transmission can be affected and no cavitation is achieved in a phenomenon known as decoupling). In this case, medium temperature varied from 28 to 35 °C during experimental tests so that

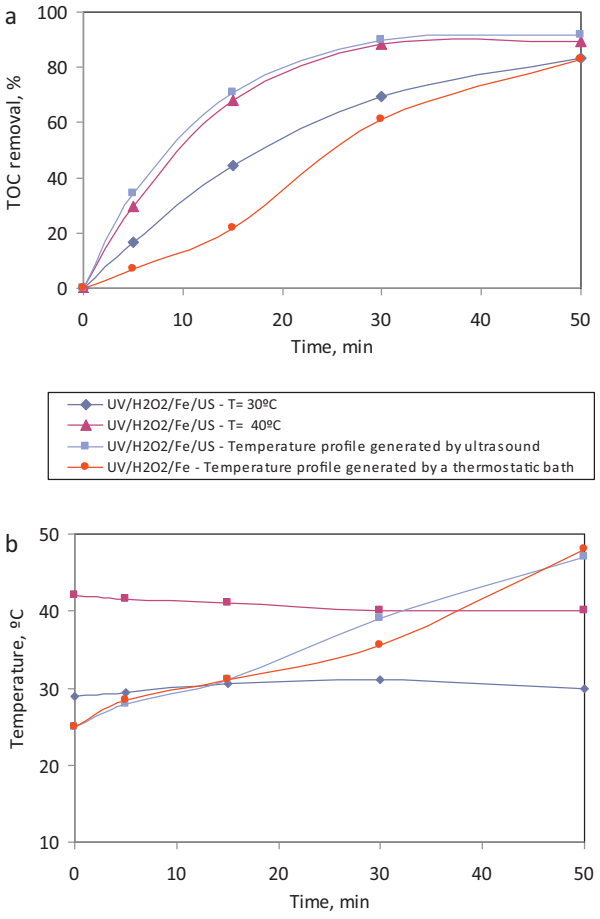

Fig. 4. Effect of temperature on the mineralization of antipyirine at optimal conditions: $[H_2O_2]$ = 1500 ppm, [Fe(II)] = 12 ppm, amplitude = 100, pulse length = 0.3 (during 15 min) and 1 later. (a) TOC removal; (b) temperature profile.

the volatilization of antypirine (boiling temperature = 260 °C) is not considered.

However, temperature may increase up to 50 °C in experiments performed under optimal sonication conditions after 50 min of reaction. It is therefore important to clarify if the improvement in mineralization kinetics is due to sonication or to an increase in kinetics due to temperature. Fig. 4a shows that an increase in temperature (from 30 to 40 °C), increases the mineralization rate of antipyirine in the absence of ultrasonic waves. In fact, results at 40 °C are very similar to those obtained under optimal conditions operating under a temperature profile generated by the use of ultrasonic waves (beginning at 25 °C and ending at 48 °C, see Fig. 4b). Thus, an additional experiment was made simulating this temperature profile with a thermostatic bath instead of using ultrasound waves. Results clearly show that the increase in temperature is not the responsible for a faster mineralization. The presence of ultrasound is required to obtain better results. This is due to the fact that high temperatures during sonication likely facilitate bubble formation by increasing the equilibrium vapour pressure, bubbles contain more vapors that cushion bubble implosion and decrease the maximum temperature achieved upon bubble collapse, reducing the cavitational effects [22]. Moreover, high temperatures can cause degassing of the liquid phase reducing the number of nuclei available for cavitation.

3.3.5. Study of synergistic effects

Several tests were performed under optimal selected conditions to determine the relative effect of each process and the synergistic

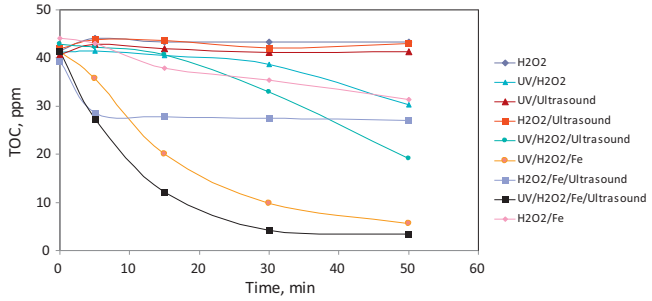

Fig. 5. TOC removal for different processes under optimal conditions.

effect of the different techniques (experiments 42–49 in Table 1). Fig. 5 compares all the experiments together with the optimal selected process studied in this work (UV/H_2O_2/Fe/US).

Mineralization of antipyrine must probably occur following a radical pathway, since H_2O_2 alone is not able to break the molecule (it is not consumed). Other combinations not generating radicals do not mineralize antipyrine. However, once the antypirine molecule has been broken, molecular H_2O_2 might react with intermediate and help in the mineralization process. This will be later studied in Section 3.4.

The use of ultrasound always improves the process due to a synergistic effect, provided that the molecule of antipyrine has been previously broken.

It can be deduced that there is a synergistic effect between sonolysis and photoFenton process (UV/H_2O_2/Fe). Thus the sonophotocatalysis (UV/H_2O_2/Fe/US) technique significantly increases TOC removal when compared with each individual technique. The synergism between the sonolysis and photoFenton process was quantified using the first order rate constants for TOC removal according to Eq. (5) [23]:

$$\text{Synergy (\%)} = \frac{k_{\text{sonophotocatalysis}} - (k_{\text{sonolysis}} + k_{\text{photoFenton}})}{k_{\text{sonophotocatalysis}}} \times 100$$

$$= \frac{0.0763 - (0.0414 + 0.002)}{0.0763} \times 100 = 45.4 \qquad (5)$$

On the other hand, the potential synergistic effect between sonocatalysis (H_2O_2/Fe/US; experiment 48) and photocatalysis (UV/H_2O_2/Fe; experiment 49) was also determined. A value of 8.78% synergy was obtained in this case.

It is confirmed that under optimal conditions, the effect is synergistic. Thus, the combined use of ultrasound and photoFenton provides an alternative and innovative water treatment method.

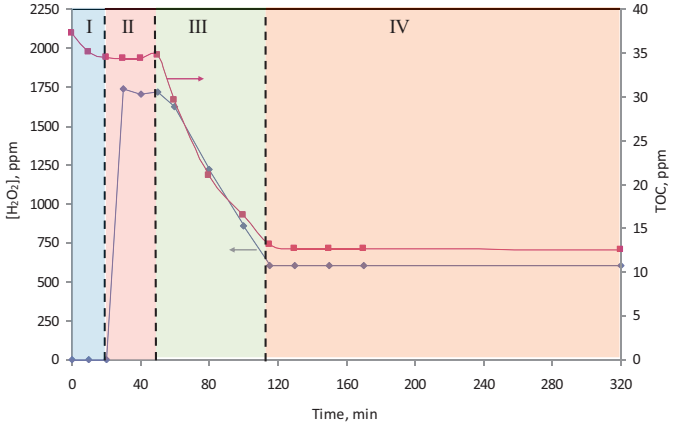

Fig. 6. Study of the radical and molecular degradation of antipyrine: TOC removal an H_2O_2 consumption.

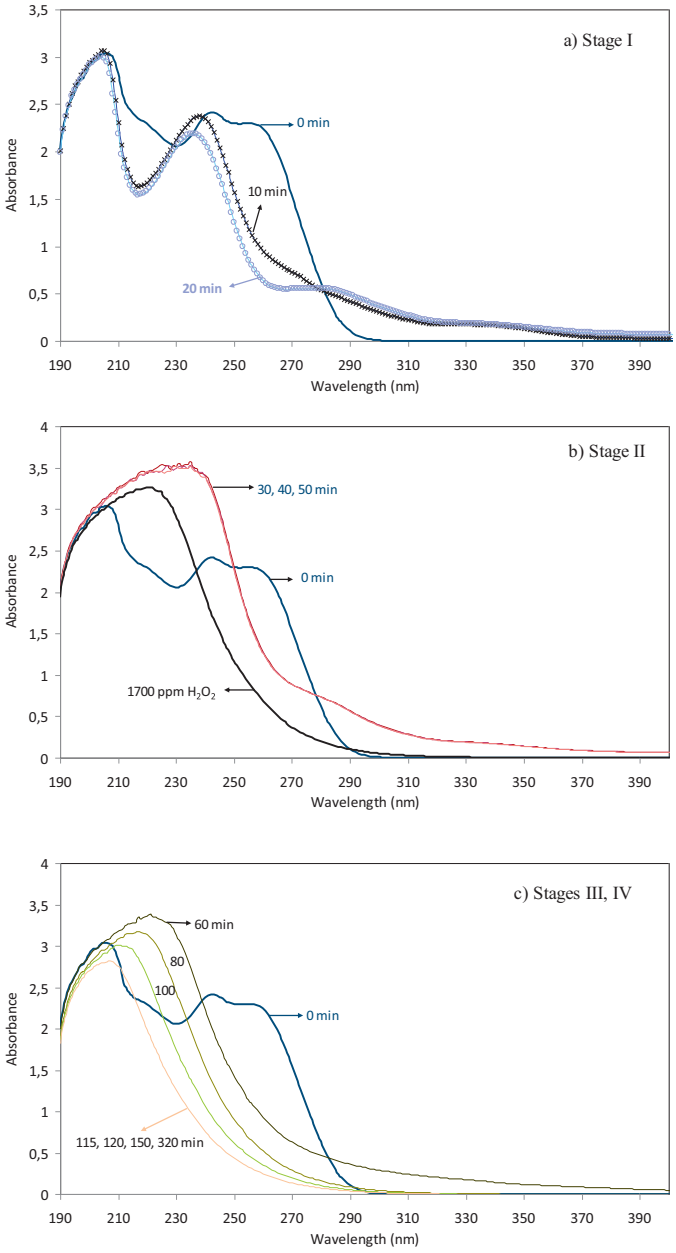

Fig. 7. Study of the radical and molecular degradation of antipyrine: UV spectra at different stages.

The expected synergism between these two modes of irradiation can be possibly attributed (in homogeneous phase) to the fact that cavitation induced radical intermediates that participate in the destruction of organic compounds [12] or to better mixing and therefore to a more efficient light absorption [24].

3.4. Degradation mechanism.

3.4.1. Determination of the reaction pathway in a UV/H_2O_2 system

Previous studies comparing photodegradation of different amine drugs in aqueous solution under simulated sunlight showed that antypirine was not photodegraded under otherwise identical conditions [25]. This was attributed to the p–π conjugation of C—N bond in the penta-heterocycle of antipyrine. The conjugation effect made the N-electrons of antipyrine become less available. The addition of H_2O_2 to the system changes this behaviour. In order

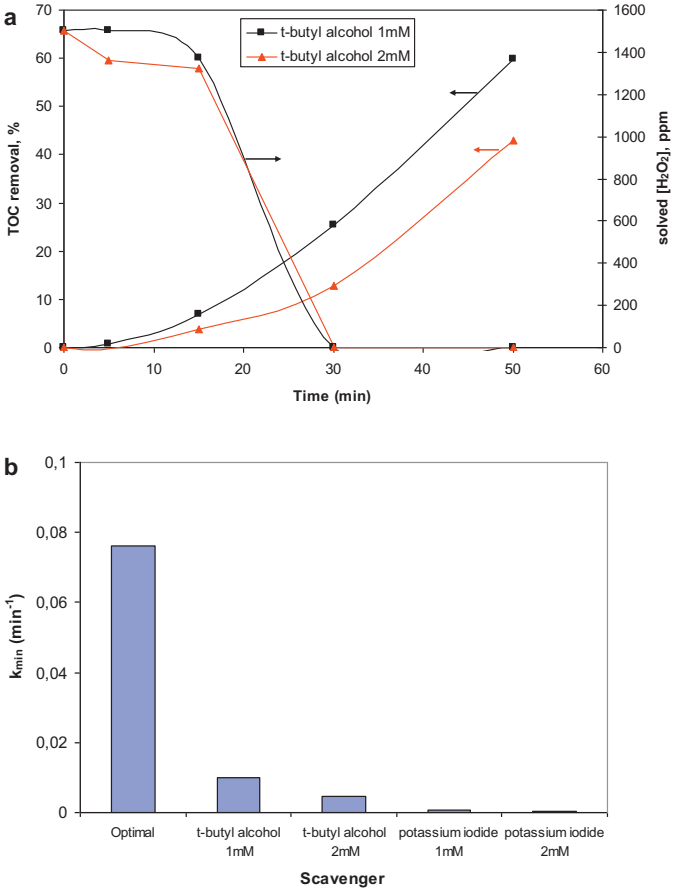

Fig. 8. Study of scavenger loaded conditions: (a) effect of t-butyl alcohol on TOC removal and H_2O_2 consumption; (b) effect of different scavengers on the mineralization rate constant.

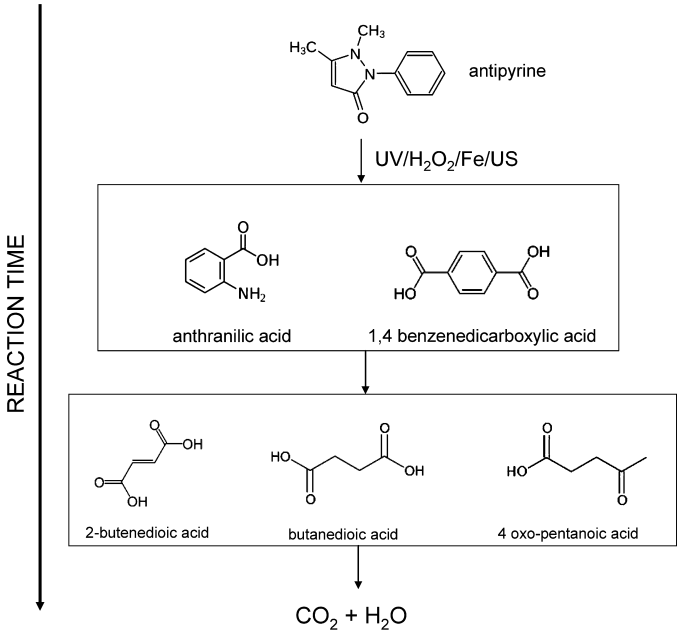

Fig. 9. Antypirine degradation pathway induced by UV/H_2O_2/Fe/US.

to determine whether the antipyirine and its degradation products were destroyed following a molecular or radical pathway in a UV/H_2O_2 system, a long test was made in four stages (without sonication) and UV-spectra were recorded to quantify antipyrine destruction. The experimental proceeding was the following:

(i) Stage I: Direct photolysis of antipyrine (during 20 min) using UV alone (no H_2O_2). It can be observed (Fig. 6) a certain mineralization. It is known that simple benzene compounds show medium intensity multiplets around 254 nm for non-conjugated derivatives, and shifted to longer wavelengths when substituents are conjugated to the aromatic system. In this case, UV radiation causes a decrease in the band at about 259 nm (Fig. 7a). According to Yuan et al. [26], antipyrine photodegradation proceeds first by the cleavage of the N—N bond of penta heterocycle leading to the formation of aromatic acids, then followed by the opening of phenyl ring to form small molecular organic acids, and these organics may be decomposed further into CO_2, justifying the observed decrease in TOC.

(ii) Stage II: Molecular degradation of antypirine (20–50 min): In this stage the UV-lamp is switched off and H_2O_2 is added to the system. It was observed that the absorption of the solution at 234 nm increased with time due to the addition of hydrogen peroxide (Fig. 7b). Degradation does not proceed further and H_2O_2 is not consumed. A significant molecular degradation of antipyirine and its intermediate products can be discarded.

(iii) Stage III: Degradation of intermediates via a radical mechanism (50–115 min). Now the UV lamp is switched on again to generate radicals and confirm the degradation of intermediate products through this via. It is observed that TOC is removed linearly and hydrogen peroxide is consumed (Fig. 6). Spectra show a decrease in all peaks, confirming the radical degradation (Fig. 7c).

(iv) Stage IV: Molecular degradation of by-products. The lamp is switched off again before TOC is completely removed to determine if final degradation products can be destroyed through a molecular mechanism. However, results show no consumption of H_2O_2 and no TOC removal (Fig. 6) or changes in spectra in this stage (Fig. 7c).

3.4.2. *Experiments of scavenger-loaded conditions*

The UV/H_2O_2/Fe/US process selected in this work is expected to generate rather more radicals that the UV/H_2O_2 system, so that the molecular via would probably be discarded. Thus, in order to confirm the main active species responsible for the mineralization of antipyrine in this system, comparison experiments of scavenger-loaded conditions were undertaken (Fig. 8).

It can be seen that the use of t-butyl alcohol stops the mineralization reaction and the consumption of hydrogen peroxide during 15 min. It is known that t-butyl alcohol readily migrate to the bubble interface and react strongly with •OH at the gas-liquid interface [27]. However, after that time H_2O_2 is consumed and TOC decreases more that 50%. Probably, the ultrasound-induced splitting of water molecules is continuously generating •OH radicals that after that time are in excess over t-butyl alcohol molecules and begin to degrade organic matter. However, it is not clear if the decrease in TOC is due to antipyrine destruction or to alcohol mineralization.

Thus, new experiments were made using KI (•OH scavenger not adding carbon to the system). It can be seen (Fig. 8b) that the use of KI completely stops reaction, confirming that the mineralization of antipyrine takes place mainly through a radical mechanism.

3.4.3. *Photodegradation byproduct identification*

Mass spectrometry was performed on the reaction products of antipyrine at different times of reaction to confirm the mechanism proposed by Yuan et al. [26]. Peaks were observed and molecular formulae were assigned to these with a maximum error of 0.2%. Structures were generated by assuming that the molecules were degradation products of antipyrine with consideration of both $[R^-H]^-$ and $[R^-Na]^-$ ions for each product R.

The main intermediates found included small concentrations of anthranilic acid and 1,4-benzenedicarboxylic acid, together with higher concentrations of 2-butenedioic acid, 4-oxo-pentanoic acid and butanedioic acid. Diantipyrylmethane was not detected. Moreover, with the increase of the reaction time, the amount of aromatic acids decreases whereas the concentration of aliphatic acids increases. According to these findings the mechanism proposed by Yuan [26], can be adapted for the UV/H_2O_2/Fe/US system with the pathway proposed in Fig. 9. Antipyrine photodegradation proceeds first by the cleavage of the N—N bond of penta-heterocycle leading to the formation of two aromatic acids, then followed by the opening of phenyl ring to form small molecular organic acids, and these organics may be decomposed further into CO_2.

4. Conclusions

- The use of a homogeneous sonophotocatalytic process (UV/H2O2/Fe/US) is an alternative and innovative method for the mineralization of antipyrine. Under the selected operation conditions ([H_2O_2] = 1500 ppm, pH = 2.7, amplitude = 100%, pulse length (cycles) = 0.3 during 15 min and then 1 after that time), 92% of TOC is removed after 50 min treating an aqueous solution containing 50 ppm of antipyrine.
- The sonophotocatalysis (H_2O_2/UV/Fe/US) technique significantly increases TOC removal when compared with each individual process. The synergism between the sonolysis and photoFenton process was quantified in 45.4%
- Different tests and comparison experiments of scavenger-loaded conditions confirm that the antipyirine photodegradation proceeds mainly through a radical mechanism probably beginning by the cleavage of the N—N bond of penta heterocycle leading to the formation of aromatic acids, then followed by the opening of phenyl ring to form small molecular organic acids that may be decomposed further into CO_2.

Acknowledgements

Financial support from JCCM (POII10-0114-3563) is gratefully acknowledged.

References

[1] S.D. Kim, J. Cho, I.S. Kim, B.J. Vanderford, S.A. Water Research 41 (2007) 1013–1021.
[2] P.H. Roberts, K.V. Thomas, Science of the Total Environment 356 (2006) 143–153.
[3] D. Bendz, N.A. Paxeus, T.R. Ginn, F.J. Loge, Journal of Hazardous Materials 122 (2005) 195–204.
[4] T.A. Ternes, Water Research 32 (1998) 3245–3260.
[5] T.A. Ternes, M. Bonerz, N. Hermann, B. Teiser, H.R. Andersen, Chemosphere 66 (2007) 894–904.
[6] E. Zuccato, D. Calamari, M. Natangelo, R. Fanelli, Lancet 355 (2000) 1789–1790.
[7] T. Deblonde, C. Cossu-Leguille, P. Hartemann, International Journal of Hygiene and Environmental Health 214 (2011) 442–448.
[8] S.S. Teske, R.G. Arnold, Reviews in Environmental Science and Biotechnology 7 (2008) 107–124.
[9] C.G. Joseph, G. Li Puma, A. Bono, D. Krishnaiah, Ultrasonics Sonochemistry 16 (2009) 583–589.
[10] A. Durán, J.M. Monteagudo, I. Sanmartín, P. Gómez, Ultrasonics Sonochemistry (2013) 011, 10.1016/j.ultsonch.2012.09.
[11] M.A. Behnajady, N. Modirshahla, S.B. Tabrizi, S. Molanee, Journal of Hazardous Materials 152 (2008) 381–386.
[12] W. Li, S. Zhao, B. Qui, Y. Du, W. Xiaohong, M. Huo, Applied Catalysis B: Environmental 92 (2009) 333–340.
[13] A. Durán, J.M. Monteagudo, M. Mohedano, Applied Catalysis B: Environmental 65 (2006) 127–134.
[14] T.J. Mason, J.P. Lorimer, D.M. Bates, Ultrasonics 30 (1992) 40–42.
[15] C.G. Joseph, G. Li Puma, A. Bono, Y.H. Taufig-Yap, D. Krishnaiah, Desalination 276 (2011) 303–309.
[16] P.R. Gogate, A.B. Pandit, Advances in Environmental Research 8 (2004) 553–597.
[17] K. Makino, M.M. Mossoba, P. Riesz, Journal of Physical Chemistry 87 (2) (1983) 1369–1377.
[18] P. Riesz, D. Berdahl, C.L. Christman, Environmental Health Perspectives 64 (1985) 233–252.
[19] M. Goel, H.Q. Hu, A.S. Mujumdar, M.B. Ray, Water Research 38 (2004) 4247–4261.
[20] G. Tezcanli-Guyer, N.H. Ince, Ultrasonics Sonochemistry 10 (2003) 235–240.
[21] S. Vajnhandl, A.M. Le MArechal, Journal of Hazardous Materials 141 (2007) 329–335.
[22] Z. Eren, Journal of Environmental Management 104 (2012) 127–141.
[23] C.G. Joseph, G. Li Puma, A. Bono, Y.H. Taufiq-Yap, D. Krishnaiah, Desalination 276 (2011) 303–309.
[24] A. Gaplovsky, J. Donovalova, S. Toma, P. Hrnciar, Chemistry List 80 (1986) 989–993.
[25] Y. Chen, C. Hu, X. Hu, J. Qu, Environmental Science and Technology 43 (2009) 2760–2765.
[26] F. Yuan, Ch. Hu, X. Hu, J. Qu, M. Yang, Water Research 43 (2009) 1766–1774.
[27] H. Ghodbane, O. Hamdaoui, Ultrasonics Sonochemistry 16 (4) (2009) 455–461.